Potential Vorticity Anomalies Associated with Squall Lines

ROLF F. A. HERTENSTEIN AND WAYNE H. SCHUBERT

Department of Atmospheric Science, Colorado State University, Fort Collins, Colorado

(Manuscript received 14 September 1990, in final form 18 January 1991)

ABSTRACT

This study involves observations and model simulations of potential vorticity anomalies in the wake of midlatitude squall lines. Using data from the Oklahoma–Kansas PRE-STORM experiment, we analyze potential vorticity fields near two squall lines—one with and one without a trailing stratiform region. From this observational analysis we suggest that squall lines *with trailing stratiform regions* can leave large, positive, midtropospheric potential vorticity anomalies in their wake. To further interpret these observations we consider a two-dimensional version of semigeostrophic theory formulated in isentropic and geostrophic coordinates, which results in a simple potential pseudodensity (inverse potential vorticity) equation. Using apparent heat source fields that model those computed diagnostically from PRE-STORM data, we find that theory does indeed predict large, midtropospheric potential vorticity anomalies for model squall lines with a trailing stratiform region but not for model squall lines that lack this feature. An interpretation of this result comes directly from the potential vorticity equation, which states that the material derivative of the potential vorticity depends on the derivative, along the vorticity vector, of the apparent heat source. In a squall line with a trailing stratiform region, large values of this derivative are found in the midtroposphere, above the lower-tropospheric evaporative cooling and below the upper-tropospheric stratiform condensational heating. This large derivative of the heating, coupled with the longer influence time associated with the width of the stratiform region, allows the potential vorticity signature of the stratiform region to dominate over the signature of the convective line. Thus, the midtropospheric mesoscale vortices often generated in the wake of squall lines are due in large part to the unique apparent heat source/sink pattern associated with the trailing stratiform region.

1. Introduction

A squall line that propagates through a conditionally unstable atmosphere excites both transient gravity-inertia waves and a more permanent balanced flow. The balanced flow is associated with the potential vorticity anomaly induced by the squall line. The sign and magnitude of this anomaly can be inferred by simply noting that the total derivative of the potential vorticity depends on the derivative (along the absolute vorticity vector) of the diabatic heat source [see Eq. (3.1) below]. If the squall line is a simple propagating diabatic source with a midtropospheric maximum, the induced potential vorticity field consists of a lower-tropospheric maximum and an upper-tropospheric minimum (Schubert et al. 1989). However, a squall line with a trailing stratiform region represents a more complicated diabatic source. The leading line is still a narrow midtropospheric source, but the trailing stratiform region represents a broad upper-tropospheric source associated with condensation and a broad lower-tropospheric sink associated with evaporation. As we shall see, this dipole in the apparent heat source of the trailing stratiform region leaves a more complicated signature in the potential vorticity field, the main feature being a midtropospheric maximum in potential vorticity. Which produces the dominant signature, the narrow, intense convective line or the broad, weak stratiform region? Although the heating of the convective line is more intense, the time interval over which it acts at a given point is relatively short; in contrast, the breadth of the stratiform region can often give sufficient time for the stratiform potential vorticity signature to dominate. In this paper we offer both observational and theoretical support for these arguments. The observational support (section 2) comes from the study of the potential vorticity fields in the wake of two PRE-STORM squall lines—one with (10–11 June 1985) and one without (26–27 June 1985) a trailing stratiform region. The theoretical support (section 3) comes from the solution of the potential vorticity and invertibility principles of an isentropic–geostrophic coordinate version of two-dimensional semigeostrophic theory.

2. Observations

a. Data and analysis

The observational component of the present study uses data from OK PRE-STORM (Oklahoma–Kansas Preliminary Regional Experiment for STORM-Cen-

Corresponding author address: Rolf Hertenstein, Department of Atmospheric Science, Colorado State University, Fort Collins, CO 80532.

tral). An overview of the measurement network, as well as details of the daily operations during this field study, can be found in Meitín and Cunning (1985) and Cunning (1986). In addition to existing NWS rawinsonde sites there were 12 supplemental PRE-STORM sites with the ability to take soundings at 90-min intervals. Using these data we have constructed cross sections (normal to the squall line) of the Rossby–Ertel potential vorticity for two squall line cases, 10–11 June and 26–27 June 1985. The Rossby–Ertel potential vorticity can be calculated from observed pressure, temperature, and winds using the quasi-static, isobaric coordinate form

$$P = \sigma_0\left\{\frac{\partial v}{\partial p}\left(\frac{\partial \theta}{\partial x}\right)_p - \frac{\partial u}{\partial p}\left(\frac{\partial \theta}{\partial y}\right)_p - \left[f + \left(\frac{\partial v}{\partial x}\right)_p - \left(\frac{\partial u}{\partial y}\right)_p\right]\frac{\partial \theta}{\partial p}\right\}, \quad (2.1a)$$

or the isentropic coordinate form

$$P = \frac{\sigma_0}{\sigma}\left[f + \left(\frac{\partial v}{\partial x}\right)_\theta - \left(\frac{\partial u}{\partial y}\right)_\theta\right], \quad (2.1b)$$

where $\sigma = -\partial p/\partial\theta$ is the isentropic pseudodensity and σ_0 is a constant reference value of σ. The forms (2.1a) and (2.1b) are equivalent, and it is a simple matter to transform from one to the other. We have found it convenient to use the isobaric form (2.1a) in the analysis of the observational data and the isentropic form (2.1b) in the theoretical analysis of section 3. In either case, Eqs. (2.1a) and (2.1b) contain a constant σ_0, giving potential vorticity the same units as vorticity. This is analogous to the introduction of a reference pressure in the definition of potential temperature in order that it have the same units as temperature. For the observational and theoretical results presented here we have chosen $\sigma_0 = 2000$ Pa K^{-1}. According to (2.1b) the potential vorticity P of an air parcel is equal to the isentropic absolute vorticity the air parcel would acquire under an adiabatic rearrangement that changed its actual pseudodensity σ to the constant reference value σ_0. With the definitions (2.1) it is natural to plot diagrams of the dimensionless quantity P/f and to think in terms of the "potential spin in units of f." For some, this may overcome the difficulty in interpretation caused by the rather obscure units associated with the usual definitions of potential vorticity.

In the application of (2.1a) to the observational data, a 3-h time composite was made for each squall line case, allowing use of more data than available for one single time. Using isochrones of the squall line leading edge determined by composite radar images, the speed and direction of movement were calculated as in Johnson and Hamilton (1988). Data for each station at times other than the central analysis time were then shifted according to the movement of the squall line. A 50-mb vertical resolution between 900 and 200 mb was chosen for analysis. Raw sounding data were interpolated to the desired level using a cubic spline routine, and a Barnes (1964) analysis scheme was used to place data on a rectangular grid for analysis or computations. In an effort to perform the analysis in the most data-rich region, we used a somewhat smaller domain than the PRE-STORM measurement network. Boundaries along 33.5° and 40°N and along 95° and 100°W were chosen. The domain was divided into 18 intervals in the east–west direction and 29 intervals in the north–south direction, giving a grid spacing of approximately 25 km. We did not correct for balloon drift in either squall line case. For the 26–27 June case, the winds aloft were relatively weak, so that there is minimal balloon drift during ascent. For the 10–11 June case, winds were stronger but inspection of the data showed maximum drift on the order of 15 km, which is small compared to the average station spacing. For ease of comparison with the model results of section 3, the observational results will also be presented in diagrams that use θ as the vertical axis.

b. 26–27 June squall line

The synoptic pattern for this squall line case featured a trough at 500 mb traveling eastward and passing north of the PRE-STORM measurement network, with weak winds at this level over most of Oklahoma and Kansas. A surface low was over Minnesota with a cold front extending through the PRE-STORM network and southwestward into New Mexico. This cold front moved across Kansas and Oklahoma between 1200 UTC on the 26th and 1200 UTC on the 27th, with the squall line forming directly along the cold front.

Composite radar images show that the squall line achieved maximum convective intensity between 2130 UTC on the 26th and 0000 UTC on the 27th (Stan Trier, personal communication). Although the convective activity was stronger at 2130 UTC, the squall line at this time was located such that a large portion of the area behind the line was outside of the PRE-STORM measurement network. As a compromise between analyzing the line during the most intense convective activity and using more available data in the network, a time of 0000 UTC on the 27th was chosen for the analysis. A composite of the base-level scans of the WSR-57 10-cm radars at Wichita and Oklahoma City for this time is shown in Fig. 1a. Vertical cross sections were taken at various locations along the length of the squall line. Details of each section varied, but the basic features of the potential vorticity fields were similar, so we present only the representative section along the line AA′ in Fig. 1a. The P/f field (Fig. 1b) shows relatively unperturbed values ahead of the squall line. Behind the squall line there are large values in the lower levels and small or even slightly negative values in the upper levels while the midlevels are less per-

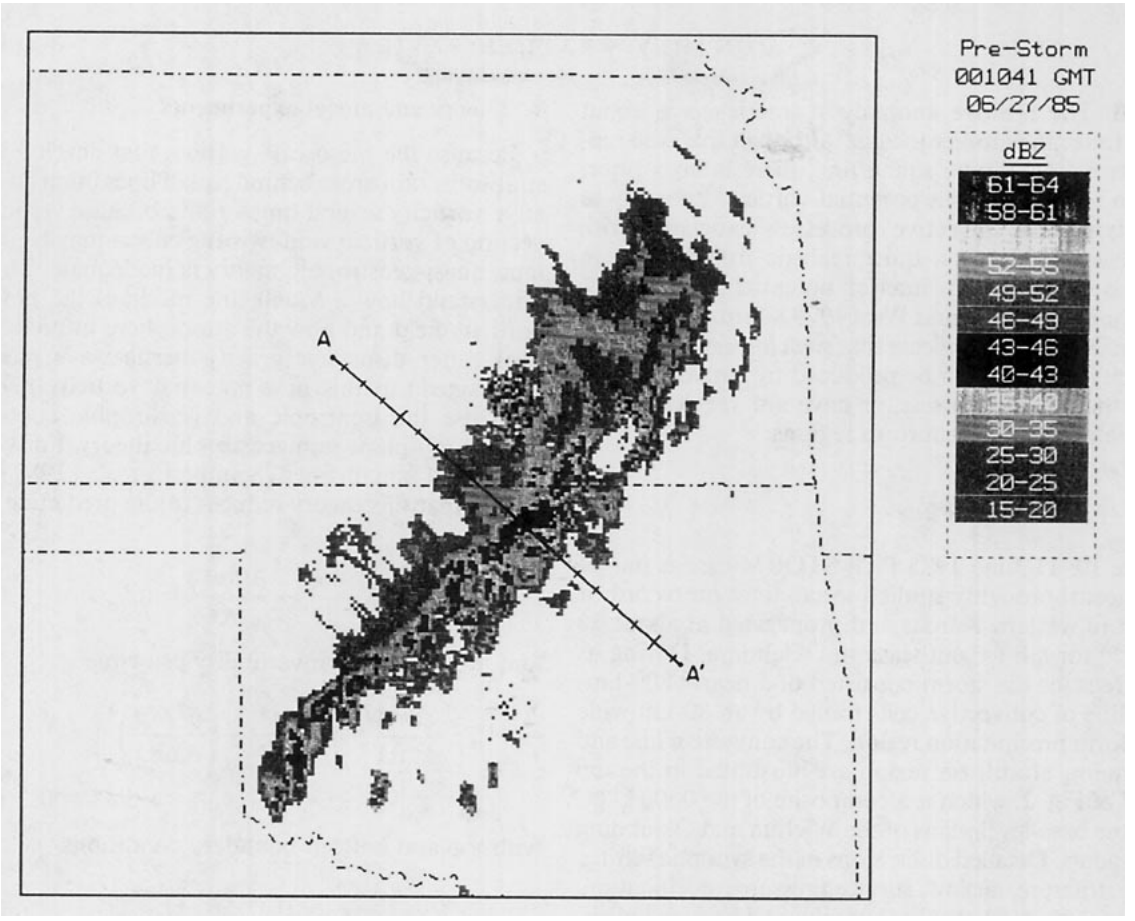

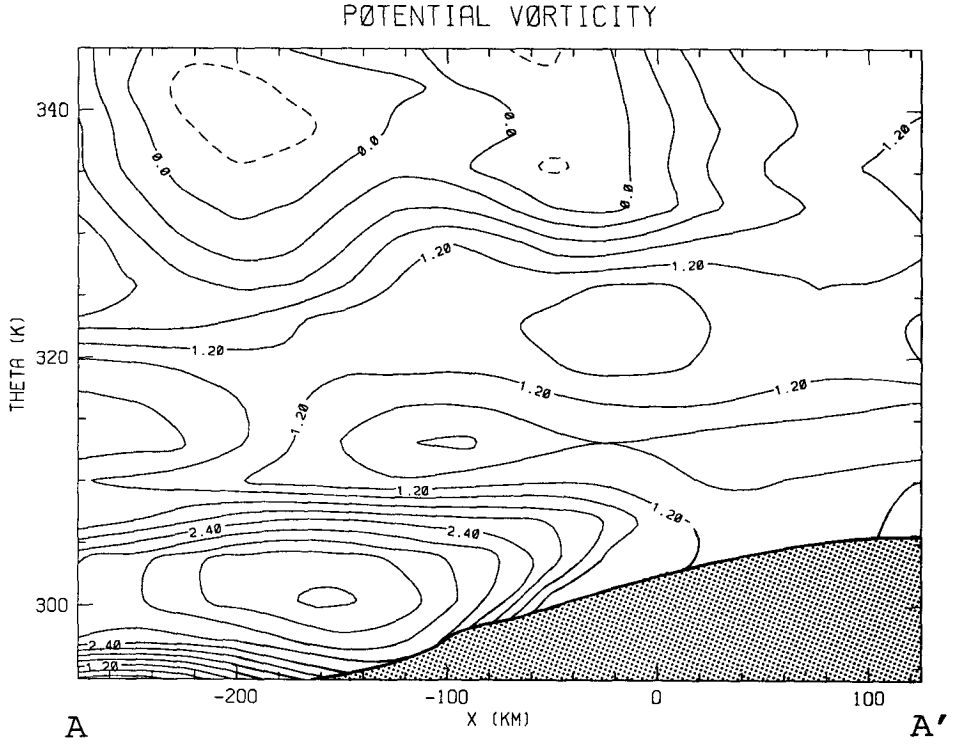

FIG. 1. (a) Composite of the 0000 UTC 27 June 1985 base-level scans of the WSR-57 10-cm radars at Wichita and Oklahoma City, with different levels of shading representing 15, 25, 35, and 45 dBZ. Also shown is the Oklahoma–Kansas PRE-STORM mesonet domain used for analyses in this study. The line AA′ indicates the location of the potential vorticity cross section shown in (b). The contours in (b) are isolines of P/f with a contour interval of 0.3. Dashed contours represent negative values. The leading edge of the squall line is located at $x = 0$.

turbed. The positive anomaly at low levels is about three times the ambient value. Although this case represents a frontal-type squall line, there is no a priori reason to attribute this potential vorticity anomaly to dry dynamical advective processes associated with frontogenesis. In fact, quite realistic fronts occur in models with uniform interior potential vorticity distributions (Hoskins and West 1979). Simulations presented in section 3 indicate that such *low-level* potential vorticity maxima can be produced by convective systems that do not possess, or have not yet developed, associated trailing stratiform regions.

c. *10–11 June squall line*

The 10–11 June 1985 PRE-STORM case is one of the most thoroughly studied squall lines on record. It began in western Kansas and propagated at about 50 km h^{-1} for 8 h to southeastern Oklahoma. During its mature stage the storm consisted of a nearly 800-km-long line of convective cells trailed by an 80-km-wide stratiform precipitation region. The convective line and the trailing stratiform region are illustrated in the top panel of Fig. 2, which is a composite of the 0600 UTC 11 June base-level scans of the Wichita and Oklahoma City radars. Detailed discussions of the synoptic setting, radar structure, airflow, surface pressure, precipitation, cloud-to-ground lightning activity, and heat and moisture budget analyses for this storm can be found in papers by Johnson and Hamilton (1988), Rutledge et al. (1988), Smull and Houze (1987), Houze et al. (1989), Augustine and Zipser (1987), Blanchard (1990), Rutledge and MacGorman (1988), and Gallus and Johnson (1991). That the stratiform region played an important role in the heat budget was suggested by Johnson and Hamilton's finding that 29% of the total rainfall occurred at the low rainfall rates associated with the stratiform precipitation. The importance of the stratiform region was confirmed by Gallus and Johnson's (1991; Figs. 8–10) heat budget calculations, which show large mid- and lower-tropospheric cooling due to evaporation, sublimation, and melting at the back edge of the radar echo where the stratiform rain was most intense.

A representative P/f cross section along the line BB′ is shown in the bottom panel of Fig. 2. In contrast to 26–27 June case this reveals a region of high potential vorticity in the *midtroposphere* with lower values above and below. The maximum midlevel positive anomaly is approximately three times the ambient value. The 10–11 June case is not an isolated example of large vorticity or potential vorticity in the stratiform rain area behind a squall line. Two other interesting cases with relative vorticity several times f were recently reported by Brandes (1990; Fig. 12) and Verlinde and Cotton (1990). In the next section we shall discuss the role of the stratiform precipitation region in generating such midtropospheric potential vorticity anomalies.

3. Theory and model experiments

Because the mesoscale vortices that develop in the stratiform rain areas behind squall lines often have relative vorticity several times f and because vertical advection of vorticity and twisting effects may be important, quasi-geostrophic theory is inadequate. Thus, to understand how a squall line modifies the potential vorticity field and how the atmosphere ultimately adjusts (after dispersive gravity-inertia wave processes have acted) to this new potential vorticity field, we shall use the isentropic and geostrophic coordinate version of f-plane semigeostrophic theory. For two-dimensional squall lines, Schubert et al. (1989) have shown that this theory reduces to the predictive equation

$$\frac{\partial \sigma^*}{\partial T} + \frac{\partial (\dot{\theta} \sigma^*)}{\partial \Theta} = 0, \tag{3.1}$$

and the diagnostic invertibility principle

$$\frac{1}{f^2}\left[\left(f^2 - \frac{\partial^2 M^*}{\partial X^2}\right)\frac{\partial^2 M^*}{\partial \Theta^2} + \left(\frac{\partial^2 M^*}{\partial X \partial \Theta}\right)^2\right] + \Gamma \sigma^* = 0, \tag{3.2a}$$

with top and bottom boundary conditions

$$\frac{\partial M^*}{\partial \Theta} = \Pi_T \quad \text{at} \quad \Theta = \Theta_T, \tag{3.2b}$$

$$\Theta \frac{\partial M^*}{\partial \Theta} - M^* + \frac{1}{2f^2}\left(\frac{\partial M^*}{\partial X}\right)^2 = 0 \quad \text{at} \quad \Theta = \Theta_B, \tag{3.2c}$$

where $\sigma^* = (f/\zeta)(-\partial p/\partial \theta)$ is the potential pseudodensity (proportional to the inverse of potential vorticity); ζ the isentropic absolute vorticity; $M^* = \theta \Pi + \phi + v_g^2/2$ the Bernoulli function; $\Pi = c_p(p/p_0)^\kappa$ the Exner function; ϕ the geopotential; $\Gamma = \kappa \Pi / p$; and the subscripts T and B denote the top and bottom of the model domain, respectively. The model is formulated in the isentropic and geostrophic coordinates $(X, \Theta, T) = (x + v_g/f, \theta, t)$, where the symbols Θ and T have been introduced so that we may use the notation $\partial/\partial\Theta$ and $\partial/\partial T$ to indicate partial derivatives with fixed X. The geostrophic wind along the squall line v_g and the mass field Π are related to M^* by

$$(f v_g, \Pi) = \left(\frac{\partial M^*}{\partial X}, \frac{\partial M^*}{\partial \Theta}\right). \tag{3.3}$$

Equations (3.1) and (3.2) form a closed system in σ^* and M^*. Fields of potential vorticity P, geostrophic wind along the squall line v_g, and Exner function Π are obtained as follows. Equation (3.1) is numerically integrated in time to obtain σ^* for a given $\dot{\theta}(X, \Theta, T)$. Since $P/f = \sigma_0/\sigma^*$, obtaining σ^* is equivalent to obtaining P. The predicted σ^* field is then used in the discretized version (Fulton 1989) of (3.2), after which

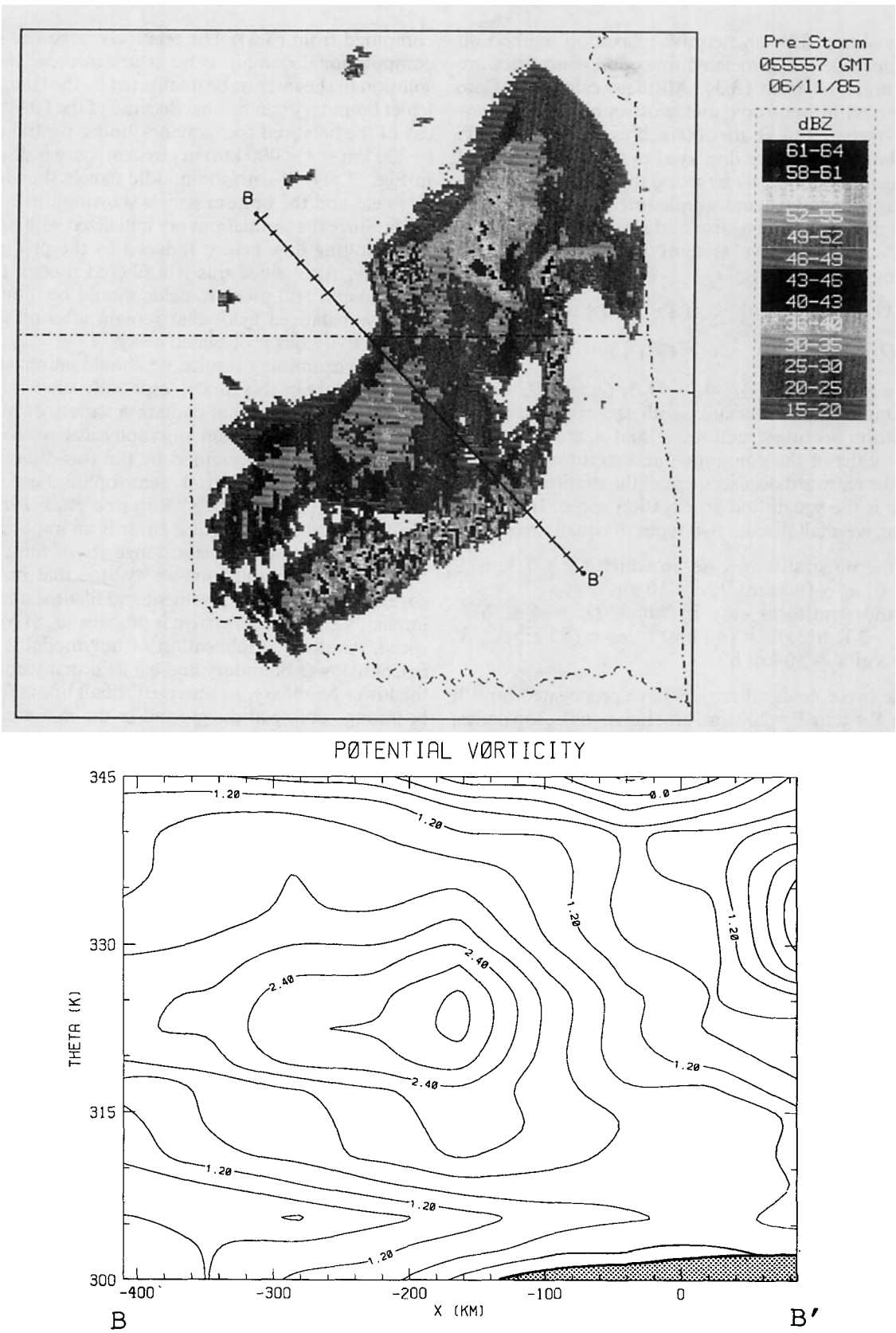

FIG. 2. Same as in Fig. 1 except for 0600 UTC 11 June 1985. The line BB′ indicates the location of the potential vorticity cross section shown in (b).

M^* is obtained by an iterative relaxation method on a single grid. The associated mass and wind fields are then obtained from (3.3). All these calculations are performed in isentropic and geostrophic space. However, once v_g and Π are obtained as functions of (X, Θ), the results can be displayed in more conventional settings such as (x, p) by using the coordinate transformation relations and simple interpolation.

To model the convective and stratiform portions of mesoscale convective systems we have chosen the heating function

$$\dot{\theta}(X, \Theta, T) = Q_c \exp[-\alpha_c^2(X - cT)^2] \sin(\pi Z) + Q_s \exp[-\alpha_s^2(X + X_s - cT)^2] \sin(2\pi Z), \quad (3.4)$$

where $Z = (\Theta - \Theta_B)/(\Theta_T - \Theta_B)$; Q_c and Q_s are the maximum rates associated with the convective and stratiform heating structures; α_c and α_s are the inverse half widths of the convective and stratiform regions; X_s is the rearward displacement of the stratiform region; and c is the squall line propagation speed. In the following we shall discuss two types of squall lines:

- the no stratiform case, in which $Q_c = 7$ K h^{-1}, $Q_s = 0$, $\alpha_c = (40 \text{ km})^{-1}$, $c = 50$ km h^{-1};
- the stratiform case in which $Q_c = 4$ K h^{-1}, $Q_s = -2$ K h^{-1}, $\alpha_c = (40 \text{ km})^{-1}$, $\alpha_s = (95 \text{ km})^{-1}$, $X_s = 45$ km, $c = 50$ km h^{-1}.

These two $\dot{\theta}$ fields, after they have propagated for 4 h from $X = 0$ to $X = 200$ km, are shown in the top panels of Figs. 3 and 4. The no stratiform case (Fig. 3) shows a simple, narrow midtropospheric heat source while the stratiform case (Fig. 4) shows, in addition, a trailing stratiform heat source at upper levels and heat sink at lower levels. The stratiform case is in approximate quantitative agreement with the heat budget calculations of Gallus and Johnson (1991) for the 10–11 June 1985 PRE-STORM squall line. It is also in qualitative agreement with the well-documented west African squall line studied by Chong and Hauser (1990) and with the review of heat budget calculations presented by Houze (1989).

The above θ fields can now be used in the integration of (3.1), once an initial condition on σ^* is given. We have assumed the initial condition is one of no geostrophic flow, so that initially $\zeta = f$ and $\sigma^* = -\partial p/\partial\theta$. The horizontally uniform initial field of $-\partial p/\partial\theta$ was taken from the 45°N, July average of the U.S. Standard Atmosphere Supplements (1966). Using this initial condition, (3.1) was integrated numerically using standard finite-difference methods on the domain $-1200 \text{ km} \leq X \leq 1200$ km, $300 \text{ K} \leq \Theta \leq 340$ K with grid spacing $\Delta X = 20$ km, $\Delta\Theta = 1$ K. The resulting σ^* field at $T = 4$ h was then used in the invertibility principle (discretized with centered second-order finite differences), which was solved iteratively for M^* on the same grid. After convergence of the iterative solution for M^*, the wind field and the mass field were computed from (3.3). The relatively large size of the computational domain is necessary in order that the solution in the interior be unaffected by the lateral Dirichlet boundary conditions. Because of the far-field decay of the balanced components, only a central region ($-200 \text{ km} < x < 400$ km) in physical space is displayed in Figs. 3 and 4, with the middle panels showing the P/f field and the bottom panels showing the v_g and p fields. Since the simulations are initialized with no flow, any resulting flow field is induced by the predicted P anomaly. Also, since this is a filtered model, the resulting wind and pressure fields should be thought of as those balanced fields that remain after all gravity wave activity has propagated away.

Before examining results, we should emphasize the simple nature of this model, especially since it is used to simulate systems that contain a variety of physical processes on scales from microphysical to synoptic. One feature not represented by the two-dimensional model is cross-line, vertical, geostrophic shear. Simulations of squall lines (e.g., Rotunno et al. 1989) indicate that cross-line vertical shear is an important aspect of the propagation and longevity of the system. In the present simulations we assume that processes governing squall line movement and lifetime are acting implicitly and that the system is propagating at constant speed. Another simplification of our model is an isentropic lower boundary and a $\dot{\theta}$ field that vanishes at the lower boundary. In observed squall lines there can be strong cooling at the ground in the rain area. This can lead to horizontal variations of potential temperature at the ground, which can also be interpreted as thin sheets of very large potential vorticity there (Hoskins et al. 1985). These additional lower boundary effects could be incorporated into our model by adopting the massless layer approach (e.g., Fulton and Schubert 1991).

Potential vorticity anomalies for the no stratiform case (Fig. 3b) show a positive P anomaly in the lower troposphere and a negative anomaly in the upper troposphere. Areas with horizontal contours near the left and right edges represent regions of undisturbed P. The maximum value of the positive anomaly is approximately two times that of the ambient P field while the minimum in the negative anomaly is roughly half the ambient value. In contrast, the P/f field for the stratiform case (Fig. 4b) shows a midtropospheric positive anomaly that has a much larger amplitude than the no stratiform case. Negative anomalies occur above and below the positive anomaly. The large P anomaly in the stratiform case can be understood by noting that differentiation of the product in (3.1) results in the term $\sigma^* \partial\dot{\theta}/\partial\Theta$, which represents a derivative of the heating along the vorticity vector. In the stratiform case this term is large in the midtroposphere, above the lower-tropospheric evaporative cooling and below the upper-tropospheric stratiform condensational heating. In addition, because of the relatively larger width of

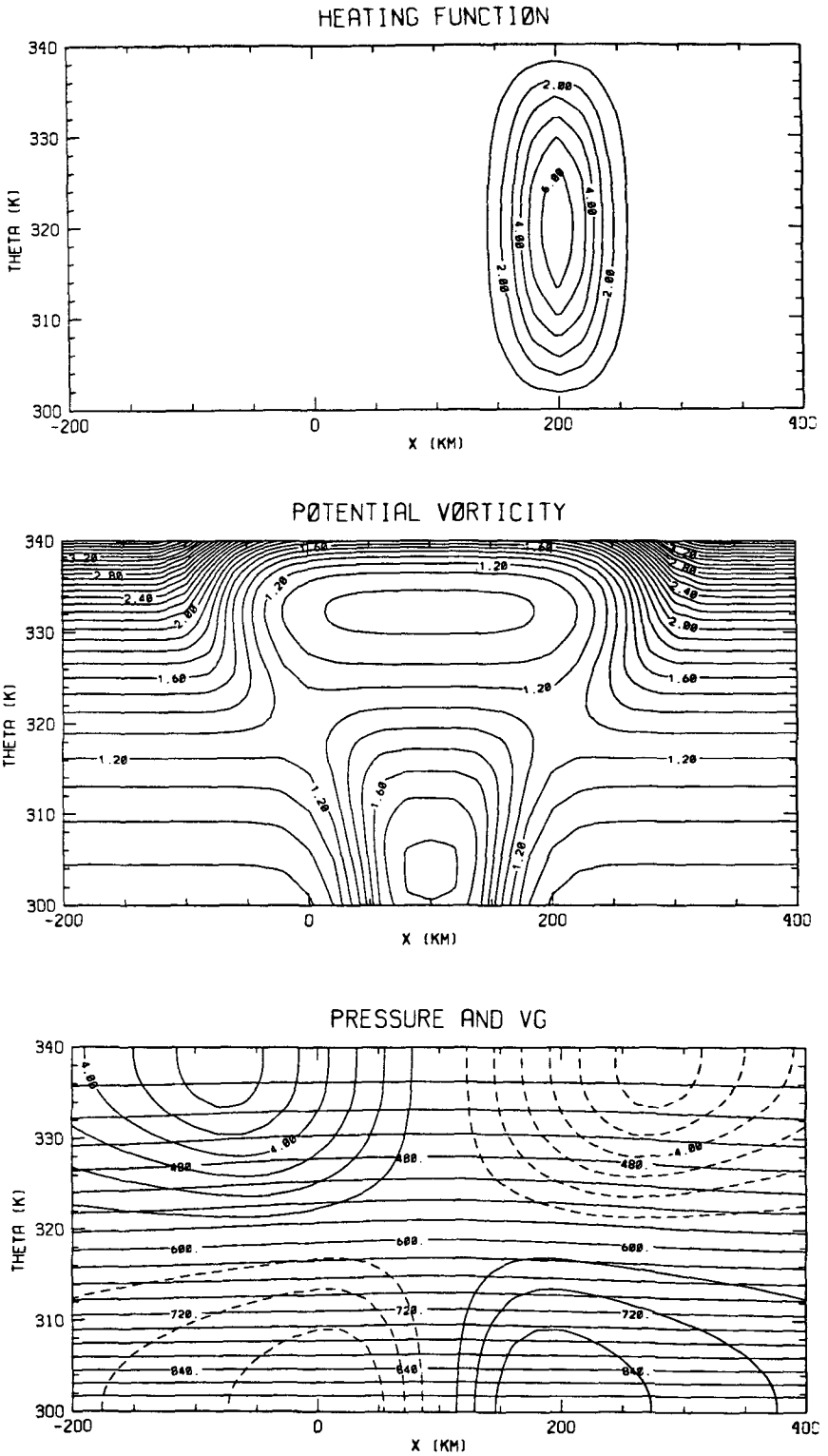

FIG. 3. (a) Heating function for the no stratiform case. For both model simulations, the squall line started at $X = 0$ and propagated to $X = 200$ km. Values are kelvins per hour with a contour interval of 1 K h^{-1}. (b) Dimensionless potential vorticity P/f in the wake of the squall line. Contour interval is 0.1. (c) Geostrophic flow along the squall line in meters per second with a contour interval of 1 m s^{-1}. Negative values represent northerly flow for a north–south aligned squall line. Also shown are isolines of pressure with a contour interval of 30 mb.

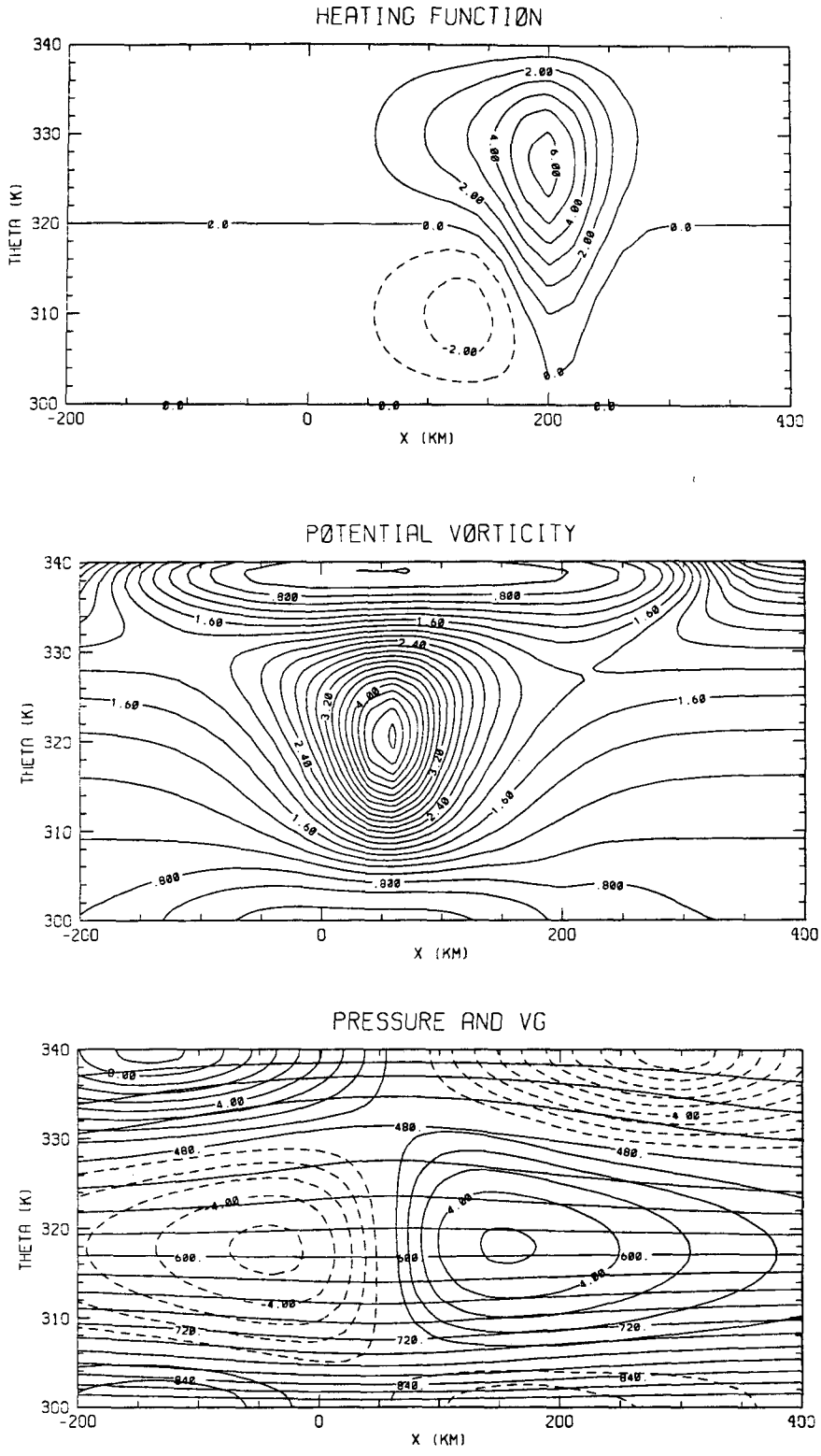

FIG. 4. Same as in Fig. 3 except for the stratiform case. Heating is indicated by solid contours while dashed lines represent cooling. Note that the contour interval for the potential vorticity field is 0.2.

the stratiform portion of the squall line, this traveling dipole of heating and cooling associated with stratiform processes has a longer time to modify the potential vorticity field.

The balanced wind and mass fields associated with these potential vorticity fields are shown in the bottom panels of Figs. 3 and 4. The no stratiform case (Fig. 3c) shows cyclonic flow in the lower levels with positive flow ahead of the system and negative flow to the rear (the simulated squall line is assumed to be aligned north–south, with southerly flow positive and northerly flow negative). Maximum speed in each branch is 3.5 m s^{-1}. In the upper troposphere the pattern is reversed with anticyclonic flow. Maximum speeds in this region are 6.5 m s^{-1}. The upper flow is stronger than the lower-level flow partly because the horizontal extent of the P anomaly is greater there (Fig. 3b) and partly because of the vertical variation of Γ. Figure 3c also shows that the pressure field is disturbed in such a way that there is destabilization at the upper levels (around 330 K). It is possible that the destabilization may establish a favorable background state for the development of the mesoscale updraft associated with the stratiform region in the mature stage of the squall line life cycle.

In contrast, the balanced flow field diagnosed for the stratiform case (Fig. 4c) shows cyclonic flow at midlevels (as anticipated from the P field) with maximum speeds of 5 m s^{-1}. Anticyclonic flow occurs above and below the cyclonic flow with a stronger upper-level anticyclone. This type of midlevel cyclonic circulation has been observed after the passage of mesoscale convective systems. For example, in their study of a long-lived mesoscale convectively generated vortex, Menard and Fritsch (1989) analyze a system in which an intense convective line quickly evolved into one with a broad stratiform region. Our model-diagnosed wind and mass fields for the stratiform case (Fig. 4c) show similarities with their analysis. The mesoscale convectively generated vortex is clearly seen in Fig. 4c as well as the cooling in the lower troposphere and warming in the middle to upper troposphere (cf., their Fig. 22). The balanced flow fields in our simulations are also in qualitative agreement with Tripoli and Cotton's (1989) conceptual MCS model, which is based on results from their two-dimensional nonhydrostatic cloud model with explicit microphysics. Thus it is likely that observed mesoscale vortices and associated temperature perturbations are the balanced wind and mass fields associated with convectively produced potential vorticity anomalies. This is one aspect of the longer term effect that organized convection has on the larger scale.

4. Concluding remarks

The observational results of section 2 show mesoscale P anomalies produced by two squall lines, the characteristics of which apparently depend on the presence of a stratiform region. The 26–27 June squall line was analyzed during its developing stage, when the system was characterized mainly by a convective line. The positive anomaly for this case was confined to the lower levels, with a negative anomaly in the upper troposphere and relatively unperturbed values in the midlevels. In contrast, the 10–11 June squall line was analyzed during its mature stage when it was characterized by both a convective line and a trailing stratiform region. The positive P anomaly for this case was located in midlevels. Upper-level patterns were less distinct in the 10–11 June case, although a weak negative anomaly was observed in the upper troposphere.

We have presented model simulations of both types of squall lines. The results of the simulations are surprisingly similar to the observations, considering the simple nature of the model. The heating profile representing the 26–27 June case (Fig. 3a) produces a simulated P anomaly with similar shape and magnitude to the observed system. The simulated anomaly does not have an unperturbed region in the midtroposphere as does the observed anomaly but rather extends from the lower-level positive anomaly to the upper-level negative anomaly. The heating profile representing the 10–11 June squall line produces a simulated P field, which also resembles the observed field. The main feature, a midlevel positive anomaly, is represented by the model, but again the simulated anomaly is vertically more extensive than observations indicate. In both squall line cases the model results are much smoother than the observational results. This is not surprising since the heating profile associated with the real squall line is more complex than the functions used as forcing in the simulations. For the simulations we have also neglected horizontal advection, which is undoubtedly an important process, especially in the veering wind conditions usually associated with severe weather. After a squall line dissipates, its potential vorticity anomaly is advected by the larger-scale flow. This process can induce vertical motion which can, in turn, set off new convection. This aspect of the problem has recently been studied by Raymond and Jiang (1990). In closing we would like to emphasize that this study has concentrated on only one aspect of mesoscale convective systems—their influence on the potential vorticity and associated wind and mass fields. Discussions of many other important physical aspects, such as gravity-wave dynamics, downdrafts, density currents, microphysics, etc, can be found in studies by Moncrieff (1978, 1989), Rotunno et al. (1988), Weisman et al. (1988), and Schmidt and Cotton (1990).

Acknowledgments. We are indebted to our colleague Richard Johnson, whose research on mesoscale convective systems has been the primary motivation for the present work. We would also like to thank Paul Ciesielski, Jennifer Francis, William Gallus, Martin Hoerling, and Mitchell Moncrieff for their reviews of

this manuscript and their helpful comments. This work was supported by the National Science Foundation primarily under Grant ATM-8814541, with partial support under Grant ATM-8518972.

REFERENCES

Augustine, J. A., and E. J. Zipser, 1987: The use of wind profilers in a mesoscale experiment. *Bull. Amer. Meteor. Soc.*, **71,** 994–1005.

Barnes, S. L., 1964: A technique for maximizing details in numerical weather map analysis. *J. Appl. Meteor.*, **3,** 396–409.

Blanchard, D. O., 1990: Mesoscale convective patterns of the southern high plains. *Bull. Amer. Meteor. Soc.*, **71,** 994–1005.

Brandes, E. A., 1990: Evolution and structure of the 6–7 May 1985 mesoscale convective system and associated vortex. *Mon. Wea. Rev.*, **118,** 109–127.

Chong, M., and D. Hauser, 1990: A tropical squall line observed during the COPT 81 experiment in West Africa. Part III: Heat and moisture budgets. *Mon. Wea. Rev.*, **118,** 1696–1706.

Cunning, J. B., 1986: The Oklahoma–Kansas preliminary regional experiment for STORM-Central. *Bull. Amer. Meteor. Soc.*, **67,** 1478–1486.

Fulton, S. R., 1989: Multigrid solution of the semigeostrophic invertibility relation. *Mon. Wea. Rev.*, **117,** 2059–2066.

——, and W. H. Schubert, 1991: Surface frontogenesis in isentropic coordinates. *J. Atmos. Sci.*, **48,** in press.

Gallus, W. A., Jr., and R. H. Johnson, 1991: Heat and moisture budgets of an intense midlatitude squall line. *J. Atmos. Sci.*, **48,** 122–146.

Hoskins, B. J., and N. V. West, 1979: Baroclinic waves and frontogenesis. Part II: Uniform potential vorticity jet flows—cold and warm fronts. *J. Atmos. Sci.*, **36,** 1663–1680.

——, M. E. McIntyre and A. W. Robertson, 1985: On the use and significance of isentropic potential vorticity maps. *Quart. J. Roy. Meteor. Soc.*, **111,** 877–946.

Houze, R. A., Jr., 1989: Observed structure of mesoscale convective systems and implications for large-scale heating. *Quart. J. Roy. Meteor. Soc.*, **115,** 425–461.

——, S. A. Rutledge, M. I. Biggerstaff and B. F. Smull, 1989: Interpretation of Doppler weather radar displays of midlatitude convective systems. *Bull. Amer. Meteor. Soc.*, **70,** 608–619.

Johnson, R. H., and P. J. Hamilton, 1988: The relationship of surface pressure features to the precipitation and airflow structure of an intense midlatitude squall line. *Mon. Wea. Rev.*, **116,** 1444–1472.

Meitín, J. G., Jr., and J. B. Cunning, 1985: The Oklahoma–Kansas preliminary experiment for STORM-Central. Vol I-Daily operations summary. NOAA Tech. Memo, ERL ESG-20, Boulder, CO 80303, 312 pp.

Menard, R. D., and J. M. Fritsch, 1989: A mesoscale convective complex-generated inertially stable warm core vortex. *Mon. Wea. Rev.*, **117,** 1237–1261.

Moncrieff, M. W., 1978: The dynamical structure of two-dimensional steady state convection in constant vertical shear. *Quart. J. Roy. Meteor. Soc.*, **104,** 543–567.

——, 1989: Analytical models of narrow cold-frontal rainbands and related phenomena. *J. Atmos. Sci.*, **46,** 150–162.

Raymond, D. J., and H. Jiang, 1990: A theory for long-lived mesoscale convective systems. *J. Atmos. Sci.*, **47,** 3067–3077.

Rotunno, R., J. B. Klemp and M. L. Weisman, 1988: A theory for strong, long-lived squall lines. *J. Atmos. Sci.*, **45,** 463–485.

Rutledge, S. A., and D. R. MacGorman, 1988: Cloud-to-ground lightning activity in the 10–11 June 1985 mesoscale convective system observed during the Oklahoma–Kansas PRE-STORM project. *Mon. Wea. Rev.*, **116,** 1393–1408.

——, R. A. Houze, M. I. Biggerstaff and T. Matejka, 1988: The Oklahoma–Kansas mesoscale convective system of 10–11 June 1985: Precipitation structure and single-Doppler radar analysis. *Mon. Wea. Rev.*, **116,** 1409–1430.

Schubert, W. H., S. R. Fulton and R. F. A. Hertenstein, 1989: Balanced atmospheric response to squall lines. *J. Atmos. Sci.*, **46,** 2478–2483.

Schmidt, J. M., and W. R. Cotton, 1990: Interactions between upper and lower tropospheric gravity waves on squall line structure and maintenance. *J. Atmos. Sci.*, **47,** 1205–1222.

Smull, B. F., and R. A. Houze, Jr., 1987: Rear inflow in squall lines with trailing stratiform precipitation. *Mon. Wea. Rev.*, **115,** 2869–2889.

Tripoli, G. J., and W. R. Cotton, 1989: Numerical study of an observed orogenic mesoscale convective system. Part 1: Simulated genesis and comparison with observations. *Mon. Wea. Rev.*, **117,** 273–304.

1966: *United States Standard Atmosphere Supplements.* United States Government Printing Office.

Verlinde, H., and W. R. Cotton, 1990: A mesoscale vortex couplet observed in the trailing anvil of a multicellular convective complex. *Mon. Wea. Rev.*, **118,** 993–1010.

Weisman, M. L., J. B. Klemp and R. Rotunno, 1988: Structure and evolution of numerically simulated squall lines. *J. Atmos. Sci.*, **45,** 1990–2013.

Zhang, D.-L., K. Gao and D. B. Parsons, 1989: Numerical simulation of an intense squall line during 10–11 June 1985 PRE-STORM. Part I: Model verification. *Mon. Wea. Rev.*, **117,** 960–994.